The DVCS Measurement at HERA

Ewelina Łobodzińska
DESY, Hamburg, Germany
Institute of Nuclear Physics, Kraków, Poland

Abstract. The recent results of the studies of Deeply Virtual Compton Scattering (DVCS) events at HERA are presented. The possibility offered by this process to gain information about skewed parton distributions (SPD) is emphasized.

1. Introduction

1.1. Motivations

The Deeply Virtual Compton Scattering process (DVCS) – shown diagrammatically in Figure 1 - is a diffractive production of a real photon in deeply inelastic scattering.

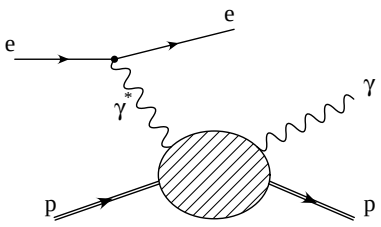

Figure 1. The DVCS process

The apparent simplicity of this process makes it a new and powerful tool to study various aspects of QCD in the field of diffraction. However, the main interest comes from the fact that DVCS gives a comparatively clean access to new parton distributions, i.e. the skewed parton distributions (SPD) [1]. SPD are the generalization of the usual parton distributions to the case where the momentum transfer to the proton is non-zero. This is illustrated in Figure 2, where two dominant QCD diagrams for DVCS are shown. The parton with the fraction x_1 of the incoming proton momentum leaves the proton and returns to it with the momentum fraction x_2. It can be noticed that in order to bring the outgoing photon onto its mass shell, the fractions of the momentum carried by the partons must be unequal (actually, x_1 - $x_2 = x_B$, where x_B is the Bjorken variable [1, 2]). DVCS is the most desirable process for extracting SPD because:

- it interferes with Bethe-Heitler process - as discussed in more detail in the next subsection - and SPD appear linearly in the interference term,

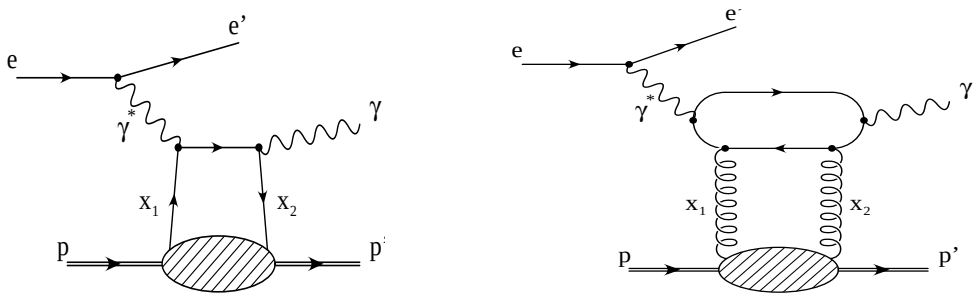

Figure 2. The two dominant QCD diagrams for DVCS.
x_1 and x_2 are the fractions of the incoming proton momentum carried by the partons.

- it has a proven QCD factorization formula, so there is a reliable theoretical basis for extracting parton distributions [2],
- it is least suppressed in Q^2 among all known exclusive diffractive processes, so it is accessible over a broad range of Q^2,
- the theoretical uncertainty connected with the process is minimized because the real final state photon is an elementary particle, so there is no need for the meson wave function as in the case of vector mesons.

During the last years, the DVCS process gained a considerable theoretical interest [2] – [8], mainly in the context of SPD. Quite recently, first observations and measurements have been reported [9]–[13].

1.2. Theoretical discussion

The reaction

$$e^+ + p \rightarrow e^+ + p + \gamma \tag{1}$$

receives contributions from both DVCS, whose origins lie in the strong interaction processes (Figure 2), and the purely electromagnetic Bethe-Heitler (BH) process (Figure 3). The total cross section for exclusive photon production described by the

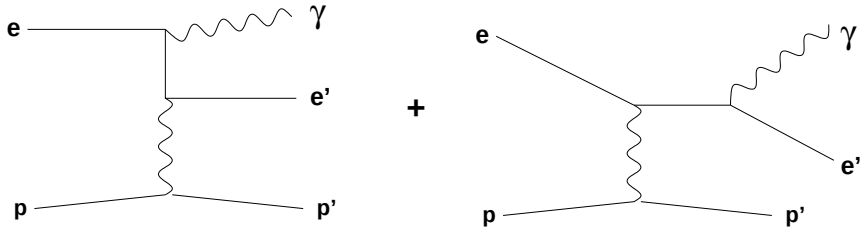

Figure 3. The Bethe-Heitler process

reaction (1) consists of three parts:

$$d\sigma^{total} = d\sigma^{DVCS} + d\sigma^{BH} + d\sigma^{interf} \tag{2}$$

where $d\sigma^{DVCS}$ is the pure DVCS cross section, $d\sigma^{BH}$ describes the BH contribution and $d\sigma^{interf}$ corresponds to interference between the BH and DVCS processes. The

BH process is well known as it depends only on QED calculations and the proton elastic form factors, so its cross section is precisely determined. It is also known that the interference term for the unpolarized positron beam is, in the leading twist approximation, proportional to $\cos\phi$, where ϕ stands for the difference in angles of the positron and the proton in the transverse scattering plane. Therefore, the interference term vanishes for all analyzes averaging over the full azimuthal angle of final states particles. In particular, in such a case the DVCS cross section can be extracted by subtracting the BH cross section from the total one. On the other hand, the measurement of the interference term gives the best access to SPD. The experimental observable to obtain SPD is the azimuthal angle asymmetry:

$$\mathcal{A} = \frac{\int_{-\pi/2}^{\pi/2} d\phi(d\sigma^{total} - d\sigma^{BH}) - \int_{\pi/2}^{3\pi/2} d\phi(d\sigma^{total} - d\sigma^{BH})}{\int_0^{2\pi} d\phi(d\sigma^{total} - d\sigma^{BH})}. \tag{3}$$

$\mathcal{A}$ describes the asymmetry for the proton and the positron to be found in the same and opposite hemispheres. It is non-zero only due to the interference term. As shown in [4, 5] the asymmetry $\mathcal{A}$ gives an access to the real part of the DVCS amplitude, which in turn allows to extract SPD.

In case of a polarized positron beam and unpolarized target the contribution to the total cross section coming from the interference term can be written in leading order (using the notation of [6]) as:

$$\begin{aligned}&(\tau^*_{BH}\tau_{DVCS} + \tau^*_{DVCS}\tau_{BH})_{pol} = \\ &\frac{4\sqrt{2}me^6}{tQx} \cdot \frac{1}{\sqrt{1-x}} \cdot e_l P_l \left[-\sin\phi \cdot \sqrt{\frac{1+\epsilon}{\epsilon}} Im\tilde{\mathcal{M}}^{1,1} \right],\end{aligned} \tag{4}$$

where τ_{BH} and τ_{DVCS} are the BH and DVCS amplitudes, $\tilde{\mathcal{M}}^{1,1}$ is the linear combination of DVCS helicity amplitudes that contributes in the polarized case, ϵ is the polarization parameter of the virtual photon while e_l and P_l denote lepton charge and polarization of the incident lepton, respectively. As it was already mentioned – in contrast to the pure BH or DVCS contributions, where the real and imaginary parts of the amplitude are mixed up and difficult to disentangle – the determination of the $\sin\phi$-moment of the asymmetry of the interference term with respect to the beam polarization provides information on the imaginary part of $\tilde{\mathcal{M}}^{1,1}$, which is directly related to SPD [6].

1.3. Monte Carlo simulations

ZEUS and H1 have each written Monte Carlo (MC) generators based on the calculations of Frankfurt, Freund and Strikman (FFS) [15], to simulate the elastic DVCS and BH processes and interference between them. Also Donnachie and Dosch (DD) [16] published their calculations of the DVCS cross section. Both these predictions provide the scattering amplitude at $t = t_{min} \simeq -m_p^2 Q^4/W^4$, where t is the squared momentum transfer to the proton, t_{min} its minimum value, m_p the proton mass and W the invariant mass of the $\gamma^* p$ system. An exponential t-dependence, $e^{-b|t|}$, is assumed.

2. Event selection

2.1. Event signatures in detector

The DVCS and BH events have a very simple signature in the detector. Since the proton escapes down the beam-pipe only the positron and the photon can be seen. In case of BH the photon is emitted from the positron lines, so the highest probability is to find both the positron and the photon in the backward‡ part of the detector. The DVCS process has a different nature, so the ratio of DVCS over BH events is expected to increase when the photon is found in the central/forward direction. The selection criteria are chosen in such a way that the detector acceptance is high and the expected contribution of DVCS to the total cross section is of the same order as that of BH. The products of the DVCS process are seen in the detector as two electromagnetic clusters : the positron emitted into a backward detector and the photon found in the central/forward calorimeter. For most of these events no track is reconstructed due to the limited acceptance of the backward tracking devices. In the BH case, events are selected with a signature identical to that of the DVCS process but, in addition, events where the photon is emitted backwards and the positron is found in the central/forward calorimeter. These are characterized by a track linked to the electromagnetic cluster in the central/forward calorimeter.

2.2. Selection cuts

The details of the selection criteria differ slightly for the ZEUS and H1 cases, however the general idea stays the same. Selected are events with:

- two electromagnetic clusters: a high energetic one detected in the backward calorimeter and one with transverse momentum > 1 GeV found in central/forward calorimeter,
- lack of any other activity above the noise threshold in the calorimeter and empty forward detectors – to eliminate dissociative events,
- no more than one track reconstructed; if the track is found, it has to be linked to one of the clusters – the cluster with the track is identified as the positron; when no track is found the backward cluster is assumed to be the positron,
- Q^2 bigger then a few GeV – to justify the use of perturbative QCD in theoretical predictions.

3. Analysis, Results and Discussion

3.1. ZEUS – the first observation of DVCS

The results of the first observation of DVCS at HERA were reported by the ZEUS Collaboration [9]. The data used for the DVCS analysis were collected during 1996-97

‡ the outgoing proton beam defines the forward direction

and correspond to an integrated luminosity of 37 pb^{-1}.

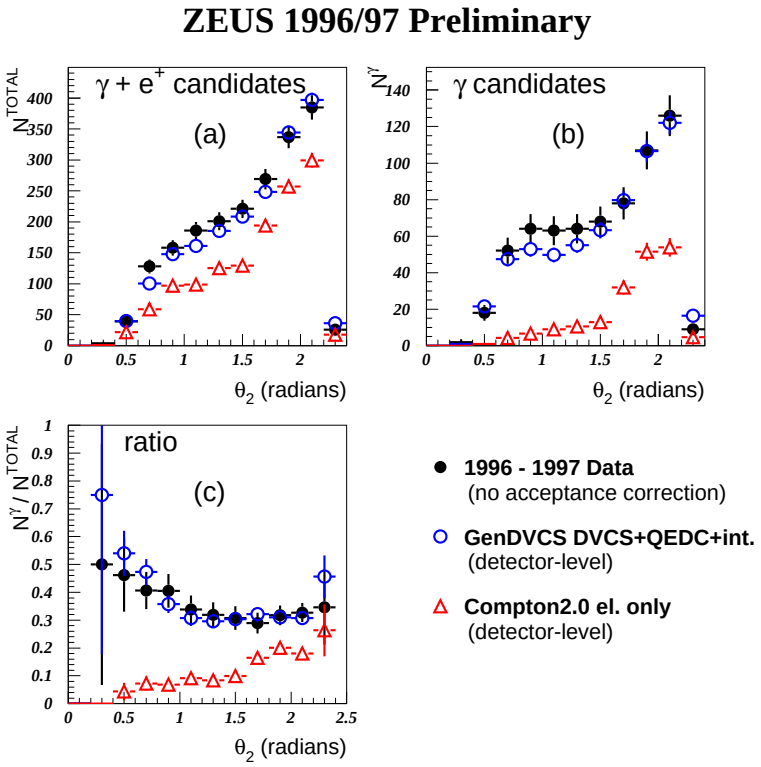

Figure 4. Distributions of the polar angle of electromagnetic cluster found in the central/forward calorimeter. (a) - all selected events, (b) - DVCS candidates only, (c) - ratio of (b) to (a). The uncorrected data (solid points) are compared to the BH (empty triangles) and DVCS+BH+interference of these two (open circles) predictions.

The selected events are plotted - Figure 4a - as a function of the polar angle of the electromagnetic cluster found in the central/forward calorimeter. The data are compared to the MC predictions for the BH process as generated by Compton2.0 [14] and to DVCS + BH + interference as predicted by the DVCS MC. All MC predictions plotted in Figure 4 are normalized to the same luminosity as the data.

Figure 4b shows similar distributions but only for DVCS candidates, i.e. the events where the electromagnetic cluster in the central/forward calorimeter is identified as a photon (no track is linked). Both plots (Figure 4a,b) indicate that the BH process alone is not able to describe the data and only the inclusion of the DVCS part brings MC into a reasonable agreement with the data.

Although the selection procedure is tailored to eliminate the inelastic events, still some contribution (expected to be of the order of 20%) remains in the selected sample. Dissociative events are not present in any of the MCs used for the analysis, so one has to keep in mind that the MC predictions have to be raised by roughly this amount in Figure 4a,b. A distribution that is found to be insensitive to the inelastic contribution is the ratio of DVCS candidates to all selected events, plotted in Figure 4c. In addition, the efficiency of finding electromagnetic cluster cancels for this distribution. It can be noticed that the conclusions drawn on the basis of two previous distributions hold also

in this case. It is now clearly seen that especially for small angle photons there is a clear deficit of events in the BH prediction.

A potential source of background arises from π^0/η production with the decay photons reconstructed in a single cluster. To investigate this background once more plots of the polar angle of the electromagnetic cluster found in the central/forward calorimeter are made, but this time also the predictions from DJANGOH (Figure 5a) and RAPGAP (Figure 5b) are overlayed. Both these MCs are expected to provide a hadronic background according to the reactions: $e^+p \to e^+p\,\pi^0\pi^0, e^+p \to e^+p\,\pi^0\eta$ etc. It can be noticed that DJANGOH predictions are similar in shape but about twice as large as RAPGAP ones.

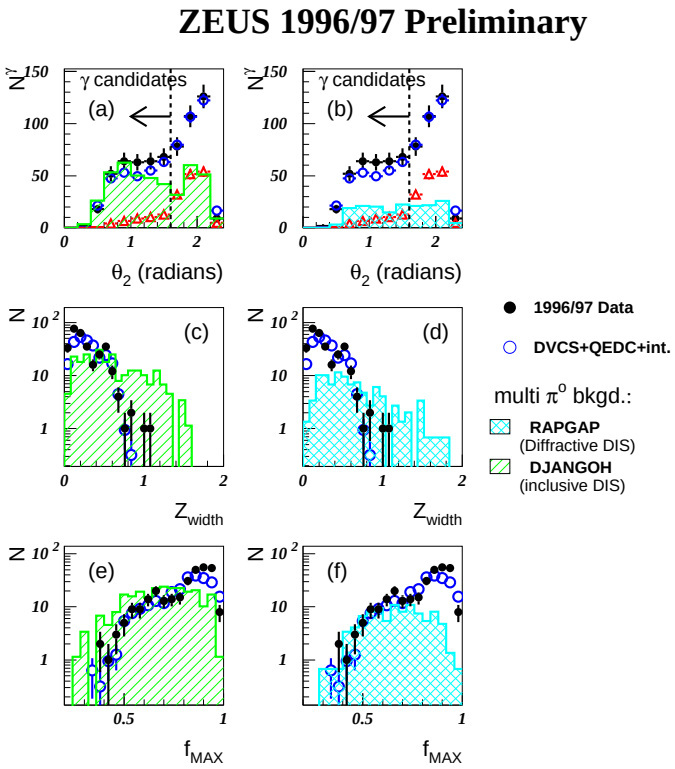

Figure 5. Distribution of (a,b) – the polar angle of electromagnetic cluster found in the central/forward calorimeter, (c,d) – the energy weighted z-position of the electromagnetic cluster expressed in units of the electromagnetic cell width, (e,f) – the fraction of the electromagnetic cluster energy carried by the most energetic cell in the cluster.

It should be stressed that both the generators (DJANGOH, RAPGAP) are high multiplicity MCs and cannot be expected to predict accurate rates for the single π^0/η production. Moreover, calculations of rates expected at HERA, based on low energy data, show that in the kinematic region where the measurement is performed one cannot expect more than a few π^0/η. Therefore, the predictions of the high multiplicity MCs seem to largely overestimate the single π^0/η background in DIS and cannot be relied on.

Another way to study the possibility of the π^0/η background is the analysis of the

shower shapes. It can be expected that the π^0/η clusters – since built by two particles – should be broader and larger, and the deposit of energy in a single calorimeter cell ought to be smaller than in case of a single photon cluster. For the purpose of this study two shower shape variables are defined:

- energy weighted average of the width of the cluster in the z–direction (z_{width})
$$z_{width} = \frac{\Sigma(\mid z_{cell} - \overline{z} \mid \cdot E_{cell})}{\Sigma E_{cell}}, \tag{5}$$
where the sum is over all cells in the electromagnetic cluster,
- the fraction of the electromagnetic cluster energy which is deposited in the most energetic cell in the cluster f_{max}
$$f_{max} = \frac{energy\ \ of\ \ the\ \ most\ \ energetic\ \ cell\ \ in\ \ the\ \ cluster}{total\ \ energy\ \ in\ \ the\ \ cluster}. \tag{6}$$

The distributions of the selected ZEUS data as a function of these two shower shape variables are shown in Figure 5c-f and compared to the π^0/η shower shapes as generated by DJANGOH and RAPGAP. These plots point out that the clusters reconstructed in the data have the same shapes as the photon clusters generated by DVCS MC. At the same time the π^0/η showers produced by DJANGOH and RAPGAP seem to be quite different since they have too small f_{max} and too large z_{width}.

The results indicate that the clusters seen in the data have different origins then those produced by π^0/η. Thus, the hadronic background from low multiplicity processes cannot account for the data excess above the BH prediction.

3.2. H1 – the first measurement of the DVCS cross section

The H1 Collaboration, made one step further and measured the DVCS cross section [10]. For this analysis H1 used the data collected in 1997 running period which corresponds to an integrated luminosity of 8 pb^{-1}.

The selected data were divided into two samples:

- control sample – characterized by the photon candidate detected in the backward calorimeter and the positron candidate in the central/forward part. This sample is dominated by the BH contribution.
- enriched DVCS sample – characterized by the positron candidate in the backward calorimeter and the photon in the central one. Both DVCS and BH contribute to this sample.

The cross section measurement is based on the enriched DVCS sample and the control part is used as a reference sample to monitor the detector performance and its simulation. In order to have control of the detector response in the same energy and angular ranges as for the enriched DVCS sample, for the calculation of kinematic variables the cluster in the central/forward calorimeter is always treated as the photon and the one in the backward calorimeter as the positron. The control sample is populated mainly by elastic BH events. However, it also contains small contributions from inelastic

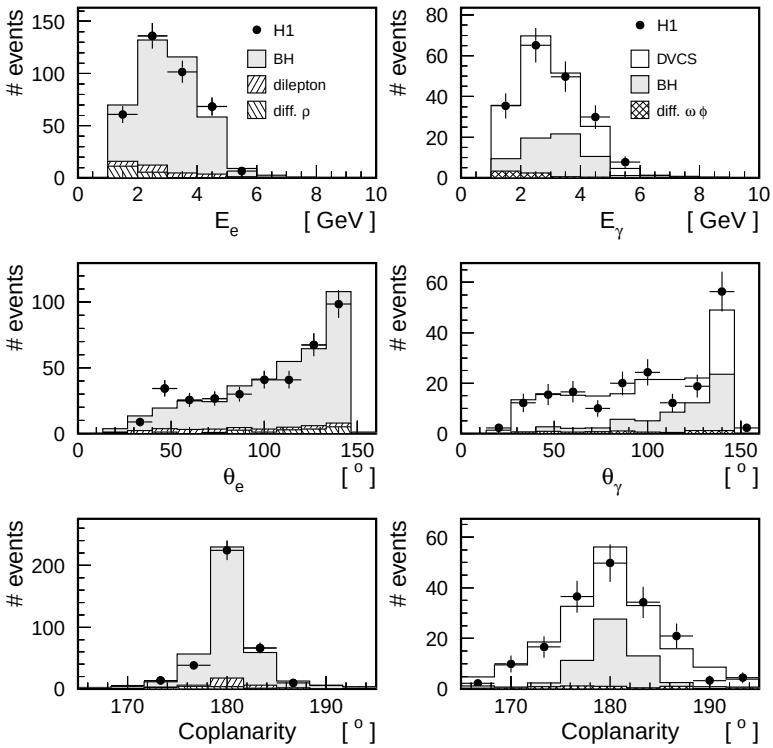

Figure 6. Distribution of (a,b) – energy of the cluster found in the central/forward calorimeter, (c,d) – polar angle of the cluster reconstructed in the central/forward calorimeter, (e,f) – coplanarity i.e. the difference of the azimuthal angle of the positron and photon candidates. Left column – events from the control sample, right column – data from the enriched DVCS sample. The data (solid points) are compared to the sum of predictions of different MC models. Plots in the left column are normalized to luminosity whereas those in the right column are normalized to the total number of events (i.e. all MCs but DVCS are normalized to the luminosity, and the total sum of events from different MC predictions is equal to the number of events from enriched DVCS sample).

BH (estimated to be $7.7 \pm 3.8\%$) as well as some events from diffractive electroproduction of ρ mesons ($\rho \to \pi^+\pi^-$) and the elastic production of electron pairs ($e^+p \to e^+e^-e^+p$). Due to the large scattering angle of the positron, the DVCS process in this sample is suppressed to negligible levels. In the left column of Figure 6 the data from the control sample are plotted and compared to the sum of MC predictions of the BH process, elastic ρ production and elastic dilepton production, all normalized to luminosity. It may be noticed that the sum of MCs provide good overall description of the data, showing that the detector response is under control and well described by the simulation.

Although the main contribution to the enriched DVCS sample comes from the elastic DVCS and BH processes also different background sources have to be considered. The contamination of inelastic DVCS and BH events has been estimated to be $16 \pm 8\%$ of the final sample. Other background sources are due to the diffractive ω ($\omega \to \pi^0\gamma$) and ϕ ($\phi \to K_l^0 K_S^0$, $K_S^0 \to \pi^0\pi^0$) production and are estimated to be 3.5%. The background arising from π^0 production in low multiplicity DIS, with the decay photons reconstructed in a single cluster, is estimated from the data and found to be negligible.

In the right column of Figure 6 various event distributions for the data from enriched DVCS sample are compared to the sum of MCs predicting contributions of all relevant processes. All MCs but DVCS are normalized to luminosity of the data. The DVCS part is normalized in such a way that the sum of contributions from different MCs is equal to the total number of events in the data. It is worth noticing that the BH prediction not only fails to describe the normalization of the data but also predicts a different shape for some distributions. In particular, the differences in shape are seen for the polar angle and coplanarity, where the latter is defined as the difference in azimuthal angle of the photon and positron clusters. The coplanarity for the data is much broader than the one predicted by the BH MC. This is attributed to the electromagnetic nature of the BH process which has a steeper t–dependence than the DVCS signal.

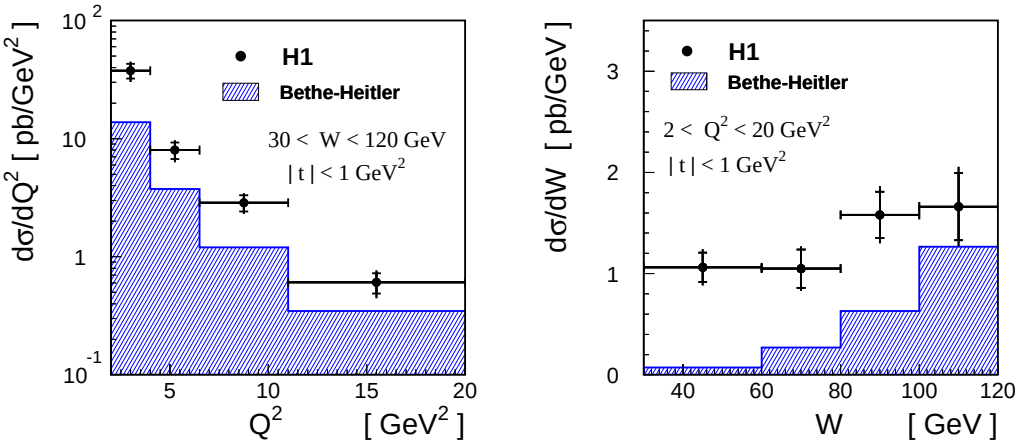

Figure 7. Differential cross section for the reaction $e^+p \to e^+p\gamma$ as a function of Q^2 (a) and W (b). The data (solid points) are plotted with statistical (inner error bar) and systematic errors added in quadrature. The hatched histogram shows the contribution of BH process.

To extract the cross section the data have been corrected for acceptance, detector effects and initial state radiation (radiation of a real photon from the positron line). Also various background contributions have been subtracted. In Figure 7 the cross section is presented differentially in Q^2 and W. The measurement is performed in the kinematic region defined by: $2 < Q^2 < 20\ GeV^2$, $30 < W < 120\ GeV$, $\mid t \mid < 1\ GeV^2$. The data are compared to the BH prediction. It is noticed that at small W values, the total cross section is dominated by the DVCS contribution, while for large W, BH is dominant. Unfortunately, the limited resolution and statistics do not allow to measure the cross section differentially in t and to extract the t-slope. Data points in Figure 7 are plotted with statistical and systematical errors added in quadrature. The total systematic error is found to be around 15%. The main contribution to this error (8%) is due to the uncertainty of the measurement of the angle of the scattered positron, because for most of the events no vertex can be reconstructed. Another significant contribution ($\sim 8\%$) comes from the estimate of the contamination of inelastic events. On the basis of the explanation given in section 1.2, the DVCS cross section is extracted from the total

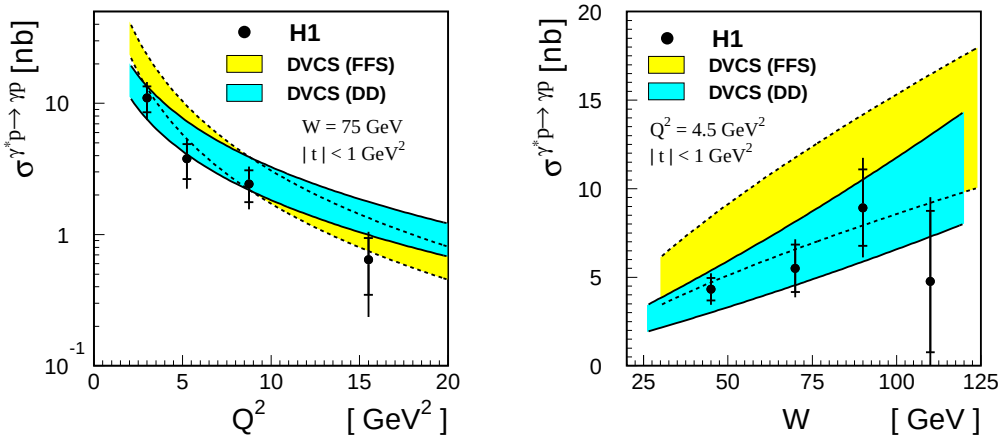

Figure 8. $\gamma^* p \to \gamma p$ DVCS cross section as a function of Q^2 (a) and W (b). The data (solid points) are plotted with statistical (inner error bar) and systematic errors added in quadrature. Theoretical predictions are shown with gray band. The band width comes from the theoretical uncertainty connected with the t-slope which is assumed to be between 5 (upper edge of the band) and 9 GeV^{-2} (lower edge).

one by subtracting the BH contribution. The result is then converted to the $\gamma^* p \to \gamma p$ DVCS cross section, plotted in Figure 8. The theoretical predictions of FFS [15] and DD [16] are also overlayed. However, due to the unknown t-slope the absolute normalization of the theoretical predictions is uncertain. The assumption of the t-slope being in the range between 5 to 9 GeV^{-2} – as suggested by the light vector meson measurements – results in the theoretical predictions seen as the bands, which lower edges correspond to the higher limit of the t-slope and the upper edges to the lower t-slope bound.

The data are, within errors, in agreement with both theoretical models.

3.3. ZEUS – the cross section measurement

Recently also ZEUS presented the results of the DVCS cross section measurement [11]. As in the previous analysis the selected events were divided into two samples: one characterized by a positron in the central calorimeter (positron sample) and the other one with a photon in that part of the detector (photon sample). The positron sample, after subtraction of a small contribution from di-electron events, was found to be in excellent agreement with BH MC predictions. The BH background was then subtracted from the photon sample using the BH MC prediction normalized according to the positron sample. Finally, the data were corrected for detector smearing and acceptance and the systematic uncertainties were analysed. The major contributions to systematic uncertainties come from the BH MC description, uncertainty in determining the hadronic background and the energy scale uncertainty.

The cross section is measured in the kinematic region defined by $Q^2 > 5\ GeV^2$, $40 < W < 140\ GeV$, $E_T^\gamma > 3\ GeV$ and $-0.6 < \eta_\gamma < 1.0$, where E_T^γ and η_γ are the transverse energy and pseudorapidity of the final state photon, respectively. In Figure 9

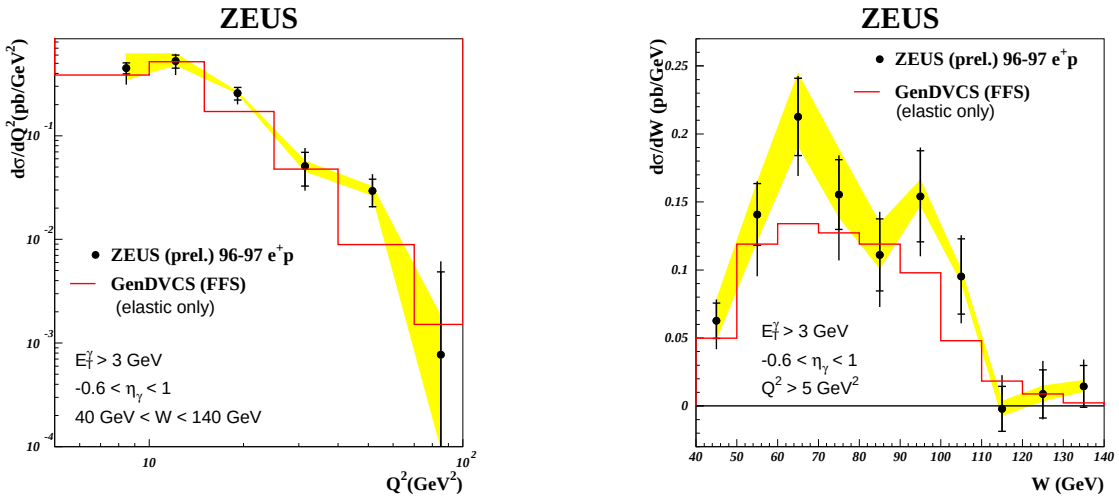

Figure 9. Differential DVCS cross section as a function of Q^2 (left) and W (right). The data (solid points) are plotted with statistical (inner error bar) and systematic errors added in quadrature. The calorimeter energy scale uncertainty, which is correlated between bins, is shown separately as the shaded band. The histogram shows the DVCS MC prediction.

the DVCS cross section is shown as a function of Q^2 and W. The data are plotted with statistical errors and systematic uncertainties added in quadrature. The energy scale uncertainty, which is correlated between bins, is shown as a band. The data are compared with the predictions of the DVCS MC. The predictions are in general agreement with the data, both in shape and normalization. However, as mentioned in section 3.1 the data include also a small (about 20%) contribution of inelastic events, so the MC predictions should be risen by roughly this amount. It can be noticed that the correction for dissociative events should improve the overall agreement between the data and DVCS MC.

3.4. HERMES – the beam-spin asymmetry in hard exclusive electroproduction of photons.

The picture of DVCS measurements at HERA cannot be complete without the recently published HERMES results [12] of the beam-spin asymmetry analysis. The data used by HERMES were collected in the years 1996-97. A longitudinally polarized positron beam and a hydrogen target were used. In contrast to the ZEUS and H1 measurements, HERMES studies observables directly connected to the interference term between the DVCS and BH processes. In Figure 10, the ϕ-dependence of the beam-spin asymmetry A_{LU} is plotted,

$$A_{LU}(\phi) = \frac{1}{\langle |P_l| \rangle} \cdot \frac{N^+(\phi) - N^-(\phi)}{N^+(\phi) + N^-(\phi)}, \tag{7}$$

where N^+ and N^- stand for the luminosity normalized yields of events with corresponding beam helicity states, $\langle |P_l| \rangle$ means the average magnitude of the beam

polarization, and the subscripts U and L denote unpolarized target and longitudinally polarized beam, respectively. Events contributing to this plot are required to have

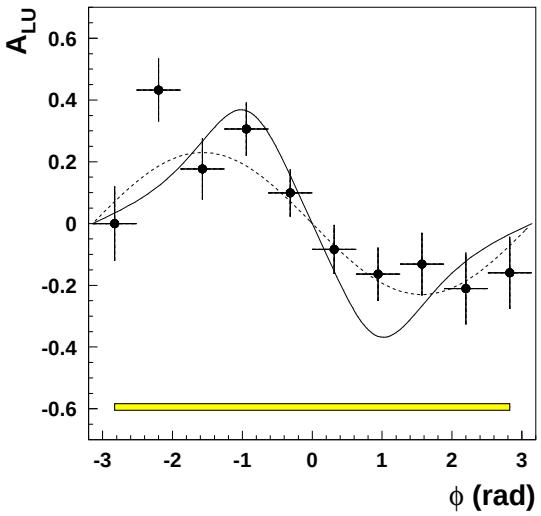

Figure 10. Beam-spin asymmetry from HERMES as a function of ϕ for the missing mass range $-1.5 < M_x < 1.7$. The dashed line shows $0.23 \cdot \sin\phi$ function and the solid one the curve calculated taking into account SPD [7].
The systematic uncertainty is represented by the error band shown at the bottom of the figure.

missing mass M_x between -1.5 and 1.7 GeV, i.e. in the range -3σ to $+1\sigma$ around the proton mass. The missing mass is defined as $M_x^2 = (q + P_p - k)^2$, where q, P_p and k denote the four momenta of the virtual photon, the target nucleon and the real photon, respectively§. The limits for the missing mass M_x required by this measurement are chosen in such an asymmetric way, in order to minimize the influence of the DIS-fragmentation background while optimizing the statistics. The data are compared to a simple $\sin\phi$ curve and to the model of Ref. [7] that takes into account SPD. The agreement between the data points and $\sin\phi$ function demonstrates that the ϕ-dependence is consistent with the expectations of equation (4). In addition, the $\sin\phi$-weighted moments are defined:

$$A_{LU}^{\sin\phi^{\pm}} = \frac{2}{N^{\pm}} \sum_{i=1}^{N} \frac{\sin\phi_i}{|P_l|_i}, \tag{8}$$

and used to analyze the beam-spin asymmetry for different missing mass bins. It turns out that the beam-spin asymmetry vanishes for higher missing masses ($M_x > 1.7$GeV), and that the sign of the $\sin\phi$ moment is opposite for the two beam helicities – which is in agreement with the expectations for the helicity dependence of the relevant DVCS-BH interference term.

§ Due to the limited momentum resolution M_x^2 may be negative and then $M_x = -\sqrt{-M_x^2}$ is defined.

4. Conclusions and Prospects

The HERA results constitute the first step in studies of the DVCS process itself, as well as in extraction of SPD by means of analysis of DVCS and its interference with BH. It is obvious that these studies do not answer all questions and do not fulfill all expectations connected with the measurement. However, the vivid theoretical interest in this process [7, 8] along with the HERA upgrade resulting in higher luminosity and the detector modifications (e.g. at H1 the improved performance of backward tracker and installation of the very forward proton spectrometer will allow for a direct t-measurement and an elastic/dissociative proton separation) give hope that at the next Ringberg workshop much more information regarding DVCS and SPD will be presented. In particular, the t-dependence of the DVCS cross section and azimuthal angle asymmetries are planned to be measured by H1 and ZEUS.

Acknowledgments

The author would like to thank the organizers for the kind invitation and perfect organization of the Ringberg workshop.

References

[1] Müller D et. al. 1994 *Fortsch. Phys.* **42** 101, Ji X 1997 *Phys. Rev. Lett.* **78** 610, Radyushkin A 1997 *Phys. Rev.* D **56** 5524, Golec-Biernat K and Martin A 1999 *Phys. Rev.* D **59** 014029
[2] Collins J C and Freund A 1999 *Phys. Rev.* D **59** 074009
[3] Ji X 1997 *Phys. Rev.* D **59** 074009, Ji X and Osborne J 1998 *Phys. Rev.* D **58** 094018, Blümlein J and Robaschnik D 2000 *Nucl. Phys.* B **581** 449
[4] Freund A 2000 *Phys. Lett.* B **472** 412
[5] Freund A and McDermott M 2001 `hep-ph/0106124`
[6] Diehl M et. al., 1997 *Phys. Lett.* B **411** 193
[7] Kivel N, Polyakov M and Vanderhaeghen M 2001 *Phys. Rev.* D **63** 114014
[8] McDermott M 2001 `hep-ph/0107224`, Freund A and McDermott M 2001 `hep-ph/0106115`, Freund A and McDermott M 2001 `hep-ph/0106319`, Korotkov V A and Nowak W D 2001 `hep-ph/0108077`
[9] Saull P R B 2000 `hep-ex/0003030`
[10] Adloff C [H1 Collaboration] 2001 *Phys.Lett.* B **517** 47
[11] [ZEUS Collaboration] 2001 *paper submitted to International Europhysiscs Conference on High Energy Physics in Budapest*
[12] Airapetian A [HERMES Collaboration] 2001 *Phys. Rev. Lett.* **87** 182001
[13] Stepanyan S [CLASS Collaboration] 2001 *Phys. Rev. Lett.* **87** 182002
[14] Courau A, Kermiche S, Carli T and Kessler P 1991 *Proc. of the Workshop on Physics at HERA (Hamburg)* vol 2 p 902
[15] Frankfurt L L, Freund A and Strikman M 1998 *Phys. Rev.* D **58** 114001 and 1999 *erratum Phys. Rev.* D **59** 119901E
[16] Donnachie A and Dosch H G 2001 *Phys. Lett.* B **502** 74